ELECTRONIC STATE ALIGNMENT, ORIENTATION, AND COHERENCE PRODUCED BY BEAM-FOIL COLLISIONS

D. A. Church

University of California
Lawrence Berkeley Laboratory
Berkeley, California 94720

INTRODUCTION

The beam-foil collision is the basic excitation means for the light source used in Beam-Foil Spectroscopy (BFS). BFS is the study of electronic level parameters and ionic structure through observation of the spectra of fast beam ions charge-changed and excited by passage through thin, self-supporting foils. Micro-Ampere beams of ions are accelerated to a known fixed energy above 10 keV, charge-to momentum analyzed, and directed through the foil to a Faraday cup. The ion-foil interaction occurs in about 10^{-14} sec., and the uniform ion velocity distributes the subsequent radiative decays of the excited levels in space downstream from the foil relative to this well-defined origin. Some of this radiation is collected, spectrally analyzed, and detected using photon-counting techniques. The radiation is generally found to have a non-isotropic spatial distribution, or alternatively to be partially polarized: both are indicative of anisotropic excitation. The spectroscopy aspects of BFS have recently been critically reviewed (1-3), and the whole field has been the subject of a continuing series of international conferences (4-6). We are concerned here with the ion-foil collision process itself; particularly those aspects which result in preferential population of certain magnetic sublevels of particular electronic levels, and the coherence effects which depend for their observation on this anisotropic excitation. The excitation is coherent when non-equal amplitudes of excitation for each sublevel have well-defined phase relations. Alternatively, the cross-sections for population of specific magnetic substates may be favored, producing incoherent non-isotropic population.

In either event, a non-stationary coherence may be induced in the wave-function subsequent to the collision by known internal or external interactions. This non-stationary coherence then results in time-dependent intensity modulations of particular polarization components of the optical decay radiation intensity. The measurement of the relative amplitudes of these intensity modulations, called quantum beats, provides a convenient method for the measurement of the excited level anisotropy. Non-isotropic population distributions in electronic levels are conveniently described by tensor multipole moment components (7). Because of the electric dipole transition selection rules $\Delta m=0,\pm 1$, only effects from tensor moments of the first three orders can be directly observed in such radiation. These moments are called respectively the line strength S, the orientation O, and the alignment A. The zeroth order moment S is a measure of the spherically symmetric excitation of the level, while the possible existence of dipole or quadrupole components follows from the particular symmetry properties of the collision geometry and the interaction (7) (See Fig. 1). The orientation and alignment components are independent, and their magnitudes are characteristic of the type and strength of the interaction producing them. The ion-foil interaction is currently not understood, so these magnitudes are measured rather than predicted. Excitation anisotropies of the outer electronic states have been studied in visible and uv radiation only for ions with incident energy less than a few MeV; the following discussion is limited to this regime. Several distinct, but related anisotropic excitation techniques will not be discussed here. They include laser excitation of fast ions (8), orientation of atoms by capture of polarized electrons during channeled passage through a magnetized crystal (9), electronic orientation of ions by hyperfine coupling to oriented nuclei (10), and angular distributions of characteristic x-ray emissions (11).

FIGURE 1

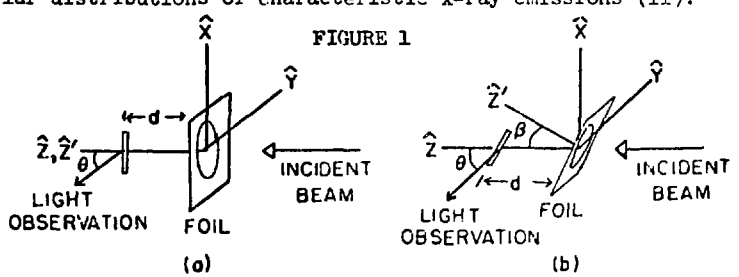

XBL 756-1611

Collision and detection geometries for (a) cylindrically symmetric, and (b) reflection symmetric beam-foil collisions. A magnetic field may be applied along $\hat{x}$ or $\hat{y}$ in (a) or $\hat{x}$, $\hat{y}$, or $\hat{z}$ in (b) to induce wavefunction coherence.

THE FOIL

The self-supporting foils usually used in beam-foil measurements are made of carbon and are thought to be polycrystalline (3). The carbon is evaporated in vacuum onto detergent coated microscope slides. The coating thickness is optically determined (12) and is customarily expressed as a surface density, with 1 $\mu g/cm^2 \approx 50\text{Å}$. Typical foil surface densities fall in the range 5-20 $\mu g/cm^2$. The non-carbon surface density component is about 1.6 $\mu g/cm^2$ independent of thickness (12). After mounting, the foil surface may have visible deviations from a plane, which change with bombardment time.

A typical beam-foil measurement is performed at pressures in the low 10^{-6} Torr range, resulting in a low degree of surface cleanliness. The excitation characteristics of surfaces freshly evaporated in vacuum initially differ from those of the typical "dirty" carbon (13) but all materials investigated relax to the "dirty" carbon values in times reciprocally related to pressure. Under ion bombardment, sufficient excited foil atoms are sputtered forward to produce observable spectra (14), up to 100 electrons per ion may be driven forward (15), and continuum photons are emitted by the foil (16). The foils exhibit certain aging characteristics after prolonged use (17) and eventually break.

The ion-foil collision differs essentially from an ion-atom collision in that the final ion state evolves from multiple interactions, with the final interaction possibly preceded by several different degrees of ionization and excitation while the beam particle is in the foil. The primary final observables (18) of the ion-foil collision are properties of the ion: its energy, direction, charge, excitation, and excitation anisotropy. The characteristics of the first four of these observables are described in the literature (19). It appears probable that the observed excited states of transmitted ions are created either at the final surface of the foil, or in the last few atomic layers of the bulk material. This we will denote by "the final surface interaction". Fig. 2 compares the excitation of two levels of fast He atoms using foil and gas collisions.

EXCITATION ANISOTROPY

Collisions with Cylindrical Symmetry

When an ion beam passes through a foil with surface normal along the beam direction, the mean collision is cylindrically symmetric, and possible alignment of the excited levels

is described by the tensor alignment component $A_o^{col} \propto \langle 3J_z^2 - J^2 \rangle$ (7). The initial density matrix elements corresponding to this alignment component are diagonal, characteristic of incoherent excitation. The linear polarization of radiation emitted from a level so aligned is described in terms of the radiation intensities emitted perpendicularly to the beam, polarized respectively parallel ($I_{\parallel}$) and perpendicular ($I_{\perp}$) to the beam direction. From these intensities, a polarization fraction $P = (I_{\parallel} - I_{\perp})/(I_{\parallel} + I_{\perp})$ may be calculated for each transition (20). If θ is the angle of observation relative to the beam axis, the angular distribution of the radiation is $I(\theta) \propto (1 - P\cos^2\theta)/(1 - P/3)$. In terms of the alignment parameter, the intensity of linearly polarized light is given by

(7) $$I_{\ell p} = \frac{1}{3}CS\{1 - \frac{h^{(2)}}{4} A_o^{col}(3\cos^2\theta - 3\sin^2\theta\cos 2\psi - 1)\} \qquad [1]$$

where C and S are constants, ψ is the angle of the linear polarizer axis relative to the beam axis, and $h^{(2)}$ is a ratio of 6j symbols determined by the angular momenta of the initial and final levels, the order of the moment, and the photon angular momentum. From this equation, one finds to first order that $P = 3h^{(2)}A_o^{col}/4$.

A measurement technique which establishes coherence between the sub-levels is useful to minimize errors due to instrumental polarizations and cascade effects from higher populated levels. Such coherence is a consequence of any interaction that begins suddenly subsequent to the collision, has a different axis of symmetry, and removes the sublevel degeneracies. Definite phase relations are then established between the sublevel wavefunctions, and interference terms with difference frequencies characteristic of the unresolved sublevel splittings produce quantum beat modulations in the emitted light intensity. The interaction may be internal, such as the fine-structure or hyperfine-structure interactions, or it may be external, such as that produced by a uniform magnetic field directed perpendicularly to the beam direction. The phase uncertainty of the ensemble is limited only by the relative time interval uncertainties between creation of the level at the foil and detection of the emitted light.

If the field strength H is fixed, the intensity of the exponential decay of a foil excited level with time constant T is then periodically modulated in time (space) $(t-t_o) = (z-z_o)/v$ according to (21):

$$I(t-t_o) = Ae^{-(z-z_o)/vT}(1 + P\cos(2\gamma_J H(z-z_o)/v)) \qquad [2]$$

If the time relative to excitation $(t-t_o) = (z-z_o)/v \equiv d/v$ is fixed, by observing light omitted at a fixed distance d from the foil while the magnetic field is swept, the modulation appears on a constant background (22). Equation [1]

exhibits this same form when $\theta=\pi/2+\omega t$ is substituted, to account for the precession of the moment. In either event, to first order, the polarization fraction P is obtained directly from the relative beat amplitude. It has been demonstrated that the period of these beats is not significantly affected by cascades (23,24), but the relative amplitude may vary with distance from the foil in the case of severe cascading.

Alignment by foil excitation is observed only when $L \geq 1$, characteristic of spin-independent excitation. Results from magnetic-field-generated beat measurements appear in Table 1. One sees that the polarization fraction is positive, and the alignment is negative, for almost all levels investigated; indeed, only certain p states have exhibited a positive alignment. The fractional alignment is generally $\lesssim 20\%$. There is a trend for the highest alignment to occur in the lower charge states, and for a given quantum number n in a specific charge state the highest L levels are generally more highly aligned at a given energy. Such tendencies are consistent with simple models for charge capture alignment (25). These trends are of course subject to the energy dependence of the alignment, which typically is not identical to that of the excitation (Fig. 2), and may be quite pronounced.

Similar coherence effects are observed in the absence of external fields when incoherently aligned L sublevels are subjected to internal interactions, such as fine-and hyperfine-structure couplings. These quantum beats appear superposed on the exponential decay of the radiated light intensity, as a function of the distance from the foil (time relative to excitation). A cosinusoidal modulation at frequencies corres-

FIGURE 2

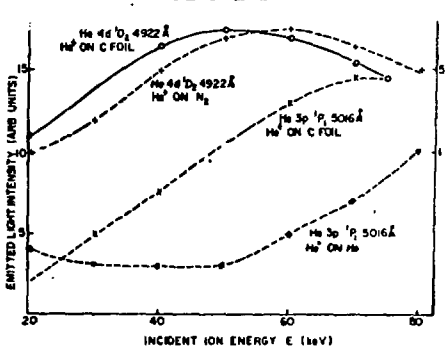

Comparison of ion-atom, ion-molecule, and ion-foil exitation for two levels of helium. The data are from Refs. 42 and 43.

TABLE I

Zeeman beat measurements of polarization fractions P of levels.

Ion	Upper Level	J	Beam Energy (KeV)	P(%)	A_o^{col}
O^+	$3p\ ^2P^o$	3/2	500	-2.4±0.2[a]	+0.032
"	$3p'\ ^2F^o$	5/2	"	4.2±0.3[a]	-0.064
"	$3p'\ ^2F^o$	7/2	"	4.1±0.3[a]	-0.073
"	$3d'\ ^2G$	7/2	"	5.5±0.5[a]	-0.096
"	$3d'\ ^2G$	9/2	"	5.5±0.5[a]	-0.107
O^{+2}	$3p\ ^3D$	2	800	2.0±0.2[a]	-0.027
"	$3p\ ^3D$	3	"	2.0±0.2[a]	-0.033
"	$3d\ ^3F^o$	3	"	3.5±0.2[a]	-0.058
"	$3d\ ^3F^o$	4	"	3.7±0.2[a]	-0.07
O^{+3}	$3p\ ^4D$	7/2	1100	2.0±0.3[a]	-0.036
"	$3d\ ^4F$	7/2	"	1.9±0.3[a]	-0.034
Ne	$2p_9\ ^2$		450	12. ±2.0[b]	-0.20
Ne^+	$3p\ ^2D$	5/2	1000	3.9±0.4[c]	-0.06
Ne^{+2}	$3p'\ ^1F$	3	"	6.0±0.4[c]	-0.10
Ar^+	$4p\ ^2P^o$	3/2	500	3.2±0.3[d]	-0.034
"	$4p\ ^2D^o$	5/2	"	3.4±0.1[d]	-0.052
"	$4p'\ ^2F^o$	5/2	"	4.8±0.8[d]	-0.073
"	$4p'\ ^2F^o$	7/2	"	6.5±0.2[d]	-0.116
Ar^{+2}	$4p'\ ^3F$	4	"	2.2±0.2[d]	-0.041

TABLE II

Beat measurements of P with relations to cross-sections.

Ion	Upper Level	Beam Energy (KeV)	P(%)	Sub-level Cross-sections
H	$2p\ ^2P$	1000	-45.0 [e]	$\sigma_o=0.38\sigma_1$
He	$3p\ ^3P$	70	10.0±1.5[f]	$\sigma_o=(1.25\pm0.15)\sigma_1$
"	$4d\ ^1D$	40	9.4±1.4[g]	$\sigma_2/\sigma_o=0.385(1+0.85\sigma_1/\sigma_o)$
"	$5d\ ^1D$	"	12.0±1.8[g]	$\sigma_2/\sigma_o=0.357(1+0.80\sigma_1/\sigma_o)$
"	$6d\ ^1D$	"	4.3±1.9[g]	$\sigma_2/\sigma_o=0.445(1+0.94\sigma_1/\sigma_o)$
"	$3d\ ^3D$	"	3.6±1.5[g]	$\sigma_2/\sigma_o=0.406(1+0.89\sigma_1/\sigma_o)$
"	$4d\ ^3D$	"	2.9±1.6[g]	$\sigma_2/\sigma_o=0.403(1+0.91\sigma_1/\sigma_o)$
"	$5d\ ^3D$	"	4.0±1.6[g]	$\sigma_2/\sigma_o=0.398(1+0.87\sigma_1/\sigma_o)$
"	$6d\ ^3D$	"	5.0±1.8[g]	$\sigma_2/\sigma_o=0.375(1+0.83\sigma_1/\sigma_o)$
Be^+	$4d\ ^2D$	300	7.8±2.0[h]	$\sigma^2+0.85\sigma_1\simeq2.7\sigma_2$
"	$5d\ ^2D$	"	3.4±1.0[h]	$\sigma_o+0.90\sigma_1\simeq2.3\sigma_2$
"	$4f\ ^2F$	"	7.5±2.0[h]	$\sigma_o+1.35\sigma_1-0.6\sigma_2\simeq3.5\sigma_3$
"	$4f\ ^2F$	"	4.6±2.0[h]	$\sigma_o+1.45\sigma_1-0.4\sigma_2\simeq3.2\sigma_3$
Be^{+2}	$2p\ ^3P$	600	1.0±0.5[h]	$\sigma_o=(1.2\pm0.1)\sigma_1$

[a]Ref. 44; [b]Ref. 22; [c]Ref. 45; [d]Ref. 46; [e]Ref. 28; [f]Ref. 30; [g]Ref. 47; [h]Ref. 48.

FIGURE 3

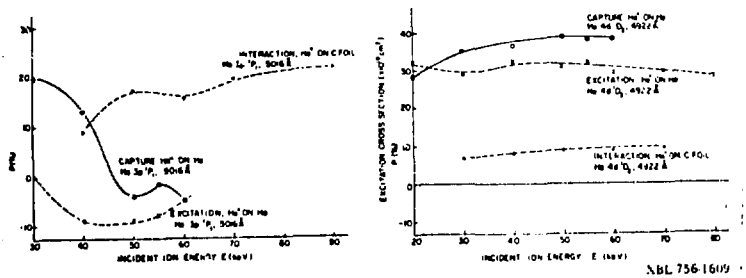

Comparison of polarization fraction results from ion-foil and ion-atom collisions. Data from Refs. 30, 31, and 41.

ponding to the separation of different J or F levels is predicted and observed (19) The initial phase of zero has been verified (26). Other formalisms (27) to analyze the data express the alignment in terms of the polarization fraction or quantum beat amplitudes, and directly relate them to the cross-sections for the population of particular m_L sublevels. Examples of data so obtained and analyzed are displayed in Table II, where the cross-sections for population of sublevels with magnetic quantum numbers $|m_L|$ are denoted σ_{m_L}.

The dependence of the alignment on the incident ion energy has been measured for only a few levels: the 2_p (28) & 3p levels (29) of H, and the 3p ^{1}P level (30) of He. One notes particularly the similarity of the H(2p) and H(3p) alignments, which exhibit broad peaks with superposed structure. In Fig. 3, some polarization fraction results from He^+-atom (31) collisions are compared with those of foil excitation.

Tilted-Foil Collisions

When the plane of the foil surface is tilted at an angle β to the beam direction (see Fig. 1-b) the collision has at most reflection symmetry in the x-z plane. Excited level moments of order $k \leq 2j$ are then in principle possible but the anisotropy directly detectable by light emission is completely described by the orientation and alignment parameters (7): Orientation $O_{1-}^{col} \propto \langle |J_y| \rangle$; Alignment $A_0^{col} \propto \langle |3J_z^2 - J^2| \rangle$; $A_{1+}^{col} \propto \langle |J_x J_z - J_z J_x| \rangle$; $A_{2+}^{col} \propto \langle |J_x^2 - J_y^2| \rangle$. Orientation of a level is defined for $J \geq \frac{1}{2}$; it is characterized by a non-zero component of angular momentum, a net magnetic moment, a population distribution among the magnetic sublevels dependent on m_L, and the emission of circularly polarized light. Alignment

components are defined for levels with $J \geq 1$; they are described by quadratic forms of the angular momentum components, no net magnetic moment, a population distribution dependent on $|m_L|$, and the emission of linearly polarized light. The orientation and alignment parameters are related to the density matrix components of the level (32). With the exception of A_o^{col}, the parameters are described by off-diagonal elements, and consequently are coherent superposition states.

It is not obvious that on the microscopic level, the gross symmetry properties represented by the tilting of the foil should affect the collision. Nevertheless, orientation manifested by a net emission of elliptically polarized radiation was observed (33) for the $3p\ ^1P$ level of He, and subsequently the effect was demonstrated to be quite general (34-36). Two observation techniques have been used to study these phenomina. The static measurement technique involves the measurement of polarized light intensity at angles of 90 degrees and 56 degrees relative to the beam direction as a function of the foil tilt angle and the beam energy (33, 37). The light was collected from a verticle beam segment, not parallel to the foil surface. The measurements are analyzed in terms of the Stokes parameters, which completely describe the polarization of the light. The dynamic measurement technique relies on coherence effects produced by an external uniform magnetic field (34, 35, 38). Quantum beats are observed as before, when the field is applied perpendicular to the beam, but the excitation coherence now permits the observation of beats when the field is applied parallel to the beam as well. The emitted light intensity is collected from a spatial region parallel to the foil surface to preserve this initial coherence.

General equations for the polarized light intensity emitted by any level (7) express static measurements in terms of the orientation and alignment parameters, and by substitution of the phase of the Larmor precession also describe the results of beat measurements (38). When a magnetic field is applied in the observation (y) direction (see Fig. 1), no orientation beats occur in circularly polarized light, demonstrating that the symmetry axis for the orientation coincides with the foil tilt axis (7, 34). All orientation and alignment parameters for the $4_d\,^1D_2$ level of He were separately determined for 40 KeV incident ion energy at the 30 deg. foil tilt angle (38). Similar measurements for the $3_p\ ^1P_1$ level of He were performed using the static measurement technique (33).

Table III shows the results of orientation measurements at particular foil tilt angles for several transitions of various ions. One sees that even with small foil tilt angles, the polarization fraction $P = (I_{\sigma+}-I_{\sigma-})/(I_{\sigma+}+I_{\sigma-})$, written

TABLE III

Orientation of atom and ion levels produced by tilted-foil collisions

Ion	Upper Level	Beam Energy (KeV)	Foil Tilt Angle (degrees)	Orientation O_{1-}^{col}
He	$3p\ ^1P$	130	30	0.027[a]
"	$3p\ ^1P$	260	25	0.053[c]
"	$4d\ ^1D$	40	30	0.008[c]
"	"	"	45	0.016[c]
"	"	"	60	0.024[c]
O^+	$3p'\ ^2F7/2$	540	25	0.014[b]
Ar^+	$4p\ ^2P3/2$	675	25	0.02 [b]
"	$4p'\ ^2F3/2$	675	25	0.022[b]
Ne^{+2}	$3p'\ ^1F7/2$	1000	30	0.008[d]
"	" 3	"	45	0.0165[d]
"	"	"	60	0.024 [d]

[a]Ref. 33; [b]Ref. 35; [c]Ref. 38; [d]Ref. 36. The orientation is calculated from the data in these references.

in terms of right and left circularly polarized light intensities emitted perpendicular to the beam, are comparable to or larger than the alignment of the same levels with an untilted foil (Tables I, II).

Measurements of the dependence of the magnitudes of the anisotropy parameters on the beam energy, foil tilt angle, or final surface material provide information about the dynamics of the interaction. Several theories for possible interactions have been suggested. A general torque interaction is expected to produce a variation of the orientation proportional to sin β, (37, 38). This is not generally observed. The torque theory of Fano (32) applies to systems which are not distorted by the interaction. In this theory, alignment is transformed to orientation by the action of an external electric field gradient. Static electric fields can also produce such a transformation (39, 40). Eck has proposed and worked out for a $^1P_1$ level a theory in which the Stark effect produced by electric fields near the foil surface produce the orientation (39). He predicts an orientation O_{1-}^{col} varying as sin 2β. The total polarization fraction of the emitted light is expected to remain constant as β is varied. None of these predictions are bourne out by experiment (36, 38). Also, the orientation of the He $3p\ ^1P_1$ level is found to reach a maximum when the alignment M/I drops to zero (37), but any relationships, or lack thereof, between these parameters are otherwise undefined.

FIGURE 4

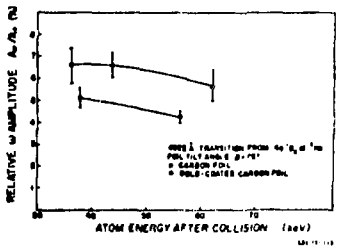

Dependence of the relative orientation signal on the material of the final surface of the foil. This dependence is found to depend on the amount of evaporated material. No reduction is found when the gold layer is on the upstream side of the foil.

The orientation interaction definitely depends on the final surface material of the foil, as Fig. 4 shows, where a thin gold layer evaporated onto the carbon foil causes a reduction of orientation (34, 41). A similar layer of aluminum produces a barely distinguishable effect, however (34, 37). Since the surfaces are presumed to be contaminated, any such observed differences may be associated with an interaction in the final foil layers, and indeed, the effect depends on the amount of evaporated material (41). The general surface field or field gradient interactions which follow are then associated with the surface contamination.

SUMMARY

The cylindrically symmetric beam-foil collision produces excitation and alignment of atom and ion levels similar, but not identical, to that resulting at comparable energies from ion-atom or ion-molecule collisions. When the foil is tilted, the macroscopic change acts on the microscopic scale to produce coherent alignment and orientation of the excited levels. The maximum beam energy range bounding this interaction has not yet been defined. The dynamic interaction which produces these effects is currently not predicted by any theory, although the dynamics of the ions subsequent to the collision are well understood. Refinement of current experimental technique can be expected to better define the final foil surface. The beam-tilted-foil collision promises to be useful in the study of ionic structure via quantum beat, radio-frequency and level-crossing spectroscopy techniques, and may provide a useful probe for certain surface interactions.

REFERENCES

1. S. Bashkin, "Beam-Foil Spectroscopy", Progress in Optics XII, E. Wolf, ed.: North-Holland, (1974), p. 288.
2. H.J. Andrä, Physica Scripta 9, 257 (1974).
3. I. Martinson and A. Gaupp, Physics Reports 15, 113 (1974).
4. S. Bashkin, ed., "Beam-Foil Spectroscopy", Gordon and Breach, New York (1968).
5. I. Martinson, J. Bromander, and H.G. Berry, ed., "Proc. Second Int. Conf. on Beam-Foil Spectroscopy", Nuc. Instrum. Meth. 90, (1970).
6. S. Bashkin, ed., "Proc. Third Int. Conf. on Beam-Foil Spectrosopy", Nuc. Instrum. Meth. 110, (1973).
7. U. Fano and J.H. Macek, Rev. Mod. Phys. 45, 553 (1973).
8. H.J. Andrä, A. Gaupp, and W. Wittmann, Phys. Rev. Letters 31, 501 (1973); H.J. Andrä, A. Gaupp, K. Tillmann, and W. Wittmann, Nuc. Instrum. Meth. 110, 453 (1973).
9. M. Kaminsky, Phys. Rev. Letters 23, 819 (1969).
10. G.D. Sprouse, R. Brown, H.A. Calvin, and H.J. Metcalf, Phys. Rev. Letters 30, 419 (1973).
11. E.H. Pedersen, S.J. Czuchlewski, M.D. Brown, L.D. Ellsworth, and J.R. Macdonald, Phys. Rev. A11, 1267 (1975).
12. J.O. Stoner, Jr., J. Appl. Phys. 40, 707 (1969).
13. K. Berkner, I. Bornstein, R.V. Pyle, and J.W. Stearns, Phys. Rev. A6, 278 (1973).
14. See e.g., H.G. Berry, I. Martinson, and J. Bromander, Phys. Letters 31A, 521 (1970); S. Bashkin, Nuc. Instrum. Meth. 90, 3 (1970).
15. C.F. Moore, W.J. Braithwaite, and D.L. Mathews, Phys. Letters 47A, 353 (1974).
16. S. Bashkin, D. Fink, P.R. Malmberg, A.B. Meinel, and S. G. Tilford, J. Opt. Soc. Am. 56, 1064 (1966).
17. See e.g., J.H. Brand, C.L. Cocke, B. Curnutte, and C. Swenson, Nuc. Instrum. Meth. 90, 63 (1970).
18. H.G. Berry, J. Bromander, and R. Buchta, Nuc. Instrum. Meth. 90, 269 (1970).
19. See reviews, Refs. 1-3, for general references.
20. I.C. Percival and M.F. Seaton, Phil. Trans. Roy. Soc. (London) 251, 113 (1958).
21. C.H. Liu and D.A. Church, Phys. Rev. Letters 29, 1200 (1972); D.A. Church and C.H. Liu, Nuc. Instrum. Meth. 110, 147 (1973).
22. C.H. Liu, S. Bashkin, W.S. Bickel, and T. Hadeishi, Phys. Rev. Letters 26, 222 (1971).
23. C.H. Liu, M. Druetta, and D.A. Church, Phys. Letters 39A, 49 (1972).
24. M. Dufay, Nuc. Instrum. Meth 110, 79 (1973).
25. R.H. Hughes, p. 103 of Ref. 4.
26. D.J. Burns and W.H. Hancock, Phys. Rev. Letters 27, 370 (1971); J. Opt. Soc. Am. 63, 241 (1973).

27. See the reviews, especially Ref. 2.
28. H.J. Andrä, P. Dobberstein, A. Gaupp, and W. Wittman, Nuc. Instrum. Meth. 110, 301 (1973).
29. D.J. Lynch, C.W. Drake, M.J. Alguard, and C.E. Fairchild, Phys. Rev. Letters 26, 1211 (1971).
30. H.G. Berry and J.L. Subtil, Phys. Rev. Letters 27, 1103 (1971); Nuc. Instrum. Meth. 110, 321 (1973).
31. F. J. DeHeer, L. Wolterbeek-Muller, and R. Geballe. Physica 31, 1745 (1965).
32. U. Fano, Phys. Rev. 133, B828 (1964); Rev. Mod. Phys. 29, 74 (1957).
33. H.G. Berry, L.J. Curtis, D.G. Ellis, and R.M. Schectman, Phys. Rev. Letters 32, 751 (1974).
34. D.A. Church, W. Kolbe, M.C. Michel, and T. Hadeishi, Phys. Rev. Letters 33, 565 (1974).
35. C.H. Liu, S. Bashkin, and D.A. Church, Phys. Rev. Letters 33, 993 (1974).
36. H.G. Berry, L.J. Curtis, and R.M. Schectman, Phys. Rev. Letters 34, 509 (1975).
37. H.G. Berry, S.N. Bhardwaj, L.J. Curtis, and R.M. Schectman, Phys. Letters 50A, 59 (1974).
38. D.A. Church, M.C. Michel, and W. Kolbe, Phys. Rev. Letters 34, 1140 (1975).
39. T.G. Eck, Phys. Rev. Letters 33, 1055 (1974).
40. M. Lombardi and M. Giroud, Compt. Rend. B266, 60 (1968).
41. D.A. Church and M.C. Michel, (to be published).
42. W.S. Bickel, K. Jensen, C.S. Neuton, and E. Veje, Nuc. Instrum. Meth. 90, 309 (1970).
43. C.E. Head and R.H. Hughes, Phys. Rev. 139, A1392 (1965).
44. D.A. Church and C.H. Liu, Physica 67, 90 (1973); Nuc. Instrum. Meth. 110, 267 (1973).
45. M. Druetta and A. Denis, Nuc. Instrum. Meth. 110, 291 (1973).
46. D.A. Church and C.H. Liu, Phys. Rev A5, 1031 (1972).
47. J. Yellin, T. Hadeishi, and M.C. Michel, Phys. Rev. Letters 30, 1286 (1973), Phys. Rev. Letters 30, 417 (1973).
48. O. Paulsen and J.L. Subtil, Phys. Rev A8, 1181 (1973); J. Phys. B7, 31 (1974).